Large particle segregation in sheared dense granular flows

Tomás Trewhela,[1,*] J. M. N. T. Gray,[2] and Christophe Ancey[1]

[1] *Laboratory of Environmental Hydraulics,*
École Polytechnique Fédérale de Lausanne, Lausanne, Switzerland

[2] *Department of Mathematics and Manchester Centre for Nonlinear Dynamics,*
University of Manchester, Oxford Road, Manchester M13 9PL, UK

(Dated: November 19, 2019)

Abstract

We studied the segregation of single large intruder particles in monodisperse granular materials. Experiments were carried out in a two-dimensional shear cell using different media and intruder diameters, whose quotient defined a size ratio that ranges from zero to unity. When sheared, the intruders segregated and rotated at different rates, which depended on their size ratio and depth. We observed greater dilation around the intruders when size ratios were closer to zero, which in turn promoted a faster segregation. However, experiments with small size ratios showed that intruder rotation was weak and local shear rates were low. On the contrary, experiments with size ratios close to unity resulted in strong intruder rotation, high local shear rates, and contraction below the intruder. Therefore, an intruder with a diameter close to that of the medium also relies on rotation to segregate. We propose that large particle segregation depends on local dilation and, to a lesser extent, the local shear rate. These observations redefine the *squeeze expulsion* mechanism [1] as two well-defined processes dependent on the size ratio and local strain rate.

I. INTRODUCTION

Polydisperse granular materials naturally segregate according to their species' size when sheared. Grain size segregation generates or favors complex phenomena such as stratification [2], fingering [3, 4], levees [5, 6], front bulging [7, 8] and channelization [9, 10]. Segregation processes affect geophysical flow characteristics [11], mixing in industrial or food processing [12] and landforms [13]. Large-particle segregation, in particular, is of great importance in helping us to comprehend debris-flow dynamics and to interpret geophysical flow deposits better [14]. In summary, grain segregation is key to understanding the dynamics of granular matter [15].

A variety of mechanisms to segregate particles have been identified and studied [16–18]. Specifically, the mechanisms of *random fluctuating sieving*, also known as *kinetic sieving* [1, 19], and *squeeze expulsion* have been studied recurrently [15]. Experimental observations and numerical simulations have described the *kinetic sieving* process precisely: this consists of small particles percolating through gaps generated by the relative movements of particle layers. The origin and nature of the *squeeze expulsion* mechanism, however, are not subject

* tomas.trewhela@epfl.ch

to a consensus. It was defined originally by Savage and Lun [1] as imbalances in the contact forces applied on an individual particle which squeeze it out of its own layer into an adjacent one. Other authors have proposed that the mechanism results from mass continuity or a net flux balance [20, 21]. Therefore, a large particle will only rise if the surrounding voids are filled with percolating smaller particles. This assumption may hold for certain cases, but small particle percolation tends to be less pressure-dependent and segregation fluxes have been found to be asymmetric [21–23]. This segregation flux asymmetry suggests that a connection between the two mechanisms may not be direct or independent of the particles size ratio or the local particle concentration.

Efforts to explain why large particles segregate have been particularly intense in recent years. Guillard *et al.* [24] proposed a scaling to define a segregation force. They found that this force was similar to a lift force and that it depended on stress distribution. However, Guillard *et al.* [24] did not address how a large intruder rises and how shear stress contributes to segregation. To address the question of why large particles segregate, van der Vaart *et al.* [25] proposed an analogy with the Saffman effect. They introduced a buoyancy-like force that depends on the size ratio to answer this question. The origin of this granular Saffman effect is similar to viscous drag, but in their work this drag is exerted by a granular flow. Recently, Staron [26] failed to observe any lift-like force under flow conditions similar to those described by van der Vaart *et al.* [25]. Staron [26] concluded that force fluctuations around the intruder should be responsible for large particle segregation. Resistance is higher towards a rigid fixed bottom, hence any force imbalance pushes the intruder upwards. An analogy to a plunging object was proposed by Staron [26], based on previous work by Hill *et al.* [27], to illustrate the previous sentence. The role of interparticle friction and rotation in particle segregation was studied by Jing *et al.* [28] through numerical simulations. Jing *et al.* [28] found that large particle segregation was supressed when interparticle friction and rotation were negligible. They proposed that the rotation of a large particle is necessary for its segregation.

Particle size segregation of a single large particle has been studied at the laboratory scale. The work by van der Vaart *et al.* [23] considered large particles segregating in a simple shear cell, but their results focused on segregation flux asymmetry. Other studies measured lift and drag forces acting over intruders in granular media [29–31]. These intruders were held fixed or moved artificially, so no direct relation could be established between their results and the segregation of a single large particle.

To study the segregation of a large particle, we used a two-dimensional shear cell filled with small particles, in which one large particle (the intruder) was placed. The cell configuration imposed a flow condition different from those used by Guillard *et al.* [24], van der Vaart *et al.* [25] and Staron [26]. In our experiments, shear was constant in depth but oscillated through time and the intruder moved freely towards the bulk free surface by the action of shear. Particle trajectories and velocity fields were determined using particle tracking velocimetry and interpolation routines, respectively. The strain rate tensor and its invariants were estimated to reveal how the granular material responded to external shear, as done in previous studies [31, 32]. Various intruder and medium diameters were used to shed light on the role of size ratio in large particle segregation.

II. METHODS

Experiments were carried out in a 5 mm-thick, two-dimensional, shear cell consisting of two parallel side-plates that rotated over axes located at their bases (Fig. 1). Cell width was set between $W = 85$ and 145 mm in $\Delta W = 15$ mm steps. A granular material between the plates was sheared by their cyclic movements. Since the side plates were parallel, the externally imposed shear rate was independent of the depth but was periodic in time. The external shear rate is expressed by

$$\dot{\gamma}_e(t) = \tan\,\theta_{max}\,\omega\cos{(\omega t)}, \tag{1}$$

where $\theta_{max} = 15°$ was the plates' maximum angle of inclination. The frequency $\omega = 2\pi/T$ was given by the period $T = 19.75$ s. Both parameters were fixed at those values for all the experiments.

Simple shear cells or boxes have been used previously to study granular and segregation processes (e.g., [23, 33, 34]). Stephens and Bridgwater [34] observed that the percolation rates and segregation mechanisms in simple shear cells were quite similar to those found in annular shear cells.

A dry granular medium made of Polyoxymethylene (POM) disks of diameter d_m and an intruder disk of the same material, but of a different diameter d_i, were placed between the cell's plates and glass panels. Three different disk diameters were employed as the surrounding media: d_m = 6, 8 and 10 mm. Only disks larger than the medium's disk diameter were used as intruders: d_i = 10, 12, 14, 18 and 20 mm. To quantify intruder rotation, a red dot was drawn on the edge of the intruders circumference.

The single intruder was initially placed in the center of the cell at a height of 4 cm,

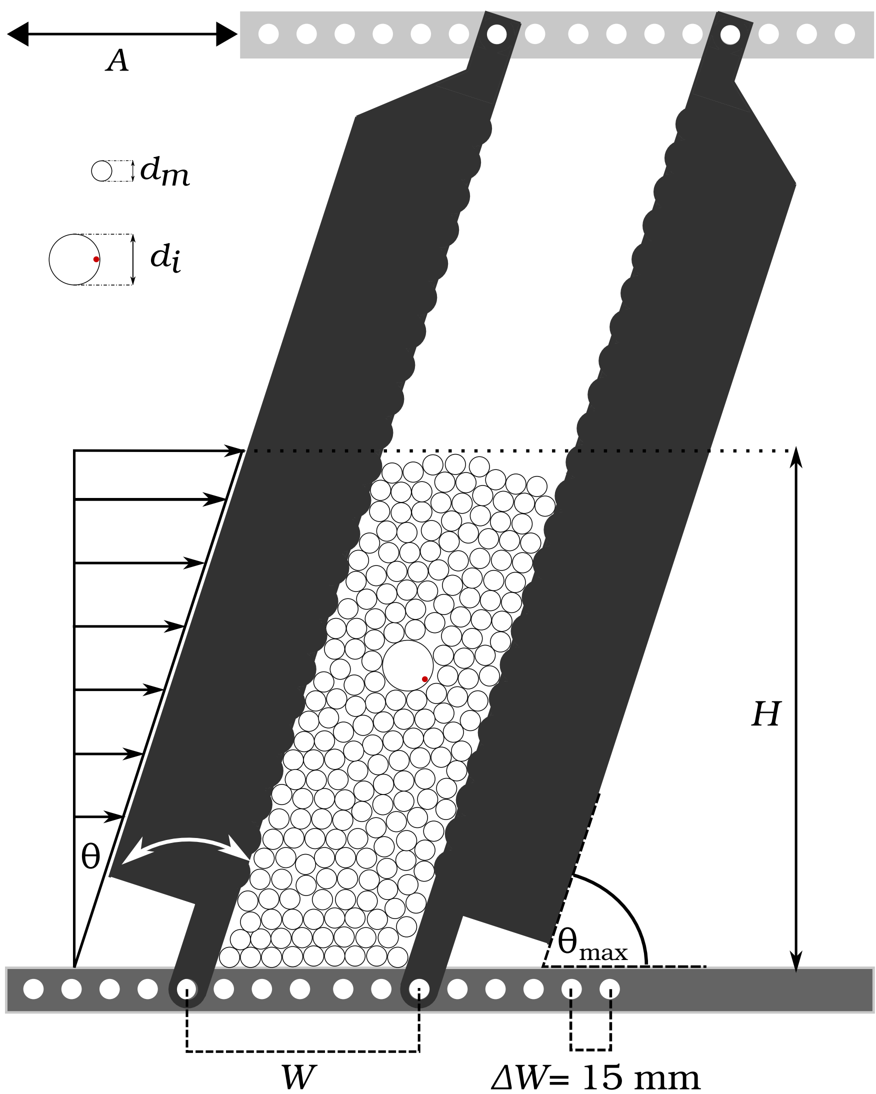

FIG. 1. Scaled schema of the 2D shear cell setup. d_m is the diameter of the disks forming the surrounding granular medium, d_i is the diameter of the intruder and A represents the amplitude generated by the cyclic movement of the plates. Bulk height $H = 19$ cm and maximum plate inclination $\theta_{max} = 15^\circ$ were the same for all experiments. Cell width W was changed for each d_m to maintain a fixed ratio of $d_m/W \simeq 9$ for all experiments.

measured from the cell bottom to the lowest point of the intruder's circumference. The cell was then filled with the smaller disks up to a height of 19 cm, creating an effective bulk height of $h = 15$ cm over the intruder. This latter condition was maintained for all experiments.

A. Image acquisition and particle tracking

Experimental run-times ranged from 15 to 70 minutes. Each experiment was recorded using a Basler acA2000-165uc camera at 4 frames per second. The position and radius of every POM disk were determined using a circular Hough-transform algorithm available on MATLAB [35]. A particle tracking algorithm was used to correlate positions to trajectories [36]. Particle positions $\boldsymbol{r}_m$ and trajectories were used to calculate particles velocities $\boldsymbol{u}_m$. Finally, spatial interpolation of the particles velocity at a certain time t enabled the calculation of the entire bulk's velocity field $\boldsymbol{u}$.

B. Intruder rotation

Red dot identification and tracking were done simultaneously to intruder tracking. The dot's position $\boldsymbol{r}_d$ and movement, relative to the intruder's position, were used to estimate the intruder's angular velocity $\boldsymbol{\Omega_i} = 2\boldsymbol{r}_d \times \boldsymbol{u}_d/d_i^2$ and the angular acceleration $\boldsymbol{\alpha_i} = d\boldsymbol{\Omega_i}/dt$. Since rotation had no preferential direction, we were interested in the magnitude of $\boldsymbol{\alpha_i}$ so its norm was considered as relevant $\alpha_i = |\boldsymbol{\alpha_i}|$.

A conditional probability $P(w_i|\alpha_i) = P(w_i, \alpha_i)/P(\alpha_i)$ was calculated to quantify the occurrence of segregation and rotation. This probability was determined from a bivariate probability distribution function (pdf) of the time series of the intruder's vertical velocity w_i and angular acceleration α_i. The bivariate pdf $P(w_i, \alpha_i)$ was calculated using MATLAB's *mvnpdf* function [35]. The second probability distribution function, for α_i alone, was determined using MATLAB's *pdf* function.

C. Strain rate tensor invariants

The strain rate tensor $\boldsymbol{D} = \frac{1}{2}(\boldsymbol{\nabla u} + \boldsymbol{\nabla u}')$ was estimated from the velocity field $\boldsymbol{u}$. A tensor decomposition determined its first invariant, the dilation [37, 38]

$$I_{\boldsymbol{D}} = \frac{1}{2}\mathrm{tr}(\boldsymbol{D}) = \frac{1}{2}(\boldsymbol{\nabla} \cdot \boldsymbol{u}), \tag{2}$$

which is proportional to the velocity field's divergence. The strain rate tensor's second invariant was obtained from the deviatoric strain rate tensor

$$II_{\boldsymbol{D}} = \left(\frac{1}{2}\mathrm{tr}(\boldsymbol{S}^2)\right)^{1/2}, \tag{3}$$

where $\boldsymbol{S} = -I_{\boldsymbol{D}}\mathbf{1} + \boldsymbol{D}$ is the deviatoric shear rate tensor. This second invariant is called the shear rate [39]. Both invariants were estimated from the velocity fields, which themselves resulted in the fields $I_{\boldsymbol{D}} = f(x, z)$ and $II_{\boldsymbol{D}} = f(x, z)$ for each time step.

To analyze the local strain rate around the intruder, we evaluated $I_{\boldsymbol{D}}$ and $II_{\boldsymbol{D}}$ on the intruder's circumference. Based on the intruder's position and diameter, we discretized the intruder's circumference in several perimeter arcs. Each arc represented a point for which the values of $I_{\boldsymbol{D}}$ and $II_{\boldsymbol{D}}$ were evaluated and extracted. This method allowed us to determine how dilated or sheared the bulk was around the intruder.

III. RESULTS

A. Vertical position

The intruder's position (Fig. 2) and bulk's velocity field were the first results obtained from the images. Near the bottom, at the beginning of the experiment, segregation was considerably slower than in upper regions. The closer the intruder got to the free surface, the faster it moved. The intruder generally showed a non-linear, depth-dependent segregation rate in all the experiments.

For all our results we used a size ratio defined as d_m/d_i, the media diameter divided by the intruder diameter. This definition provided a better fit to our results and allowed us to contain its values within a well-defined range, i.e. between 0 and 1.

As shown by Figure 2, the segregation rate $q \approx w_i = dz/dt$ increased as d_m/d_i tended to 0. These findings also held for experiments using larger medium diameters ($d_m = 8$ and 10 mm). A laddering, almost step-wise ascent, was observed in these cases, especially in the $d_m = 10$ mm medium experiments.

All the intruders demonstrated oscillatory vertical movement. Indeed, due to the plates' cyclic movement, the intruders moved upwards and downwards when the bulk was sheared. This movement could be interpreted as noise relative to an average vertical position during a cycle. Cyclical vertical movement was observed throughout the entire experiment and exhibited the same amplitude, independent of z. The magnitude of this movement did not change between experiments, even when different intruder diameters were used, as shown in Figure 2. It is important to note that the bulk media were sheared and unsheared cyclically, so the oscillatory vertical movement was the result of the setup.

An exponential law $z(t) \approx a_i e^{b_i t}$ was fitted to the intruder position, as shown in Figure 2. Initially, we tried to fit a quadratic law $z(t) \approx at^2 + bt + c$, but then the segregation rate $q \approx dz/dt$ would have required a linear fit of the type $at + b$, which was not the case. Based on the exponential fit, it was possible to collapse the results for the experiments with $d_m = 6$ mm (Fig. 2(b)). This analysis was done under the supposition that the a_i and b_i parameters were linear functions of size ratio, i.e. $a_i = m_a(1 - d_m/d_i)$ and $b_i = m_b(1 - d_m/d_i)$ (Fig. 2(a) and 2(b)). The selected functions were consistent with the no segregation condition, when $d_m/d_i = 1$. The experimental results, normalized by the fit parameters a_i and b_i, and replaced by the suggested linear fits, are shown in inset (c) of Figure 2. A good agreement was found though the role of a_i in segregation remains unclear, other than, it was related to the intruder's initial position.

Because no *kinetic sieving* mechanism was observed using the 2D shear cell configuration, we do not show any results on the percolation of small intruders through granular media made of large disks. We observed that when a single smaller intruder was introduced into the cell, it did not percolate down through the bulk. Small disks moved erratically on top of the upper layer until they found lateral gaps generated by the plate roughness, which we considered bias. We removed these experiments from our results.

We estimated a final segregation time t_f for each experiment. This was defined as the time necessary for the intruder to rise from its initial position to the top layer of particles. We normalized time t by t_f and we normalized the vertical position z by the effective bulk height

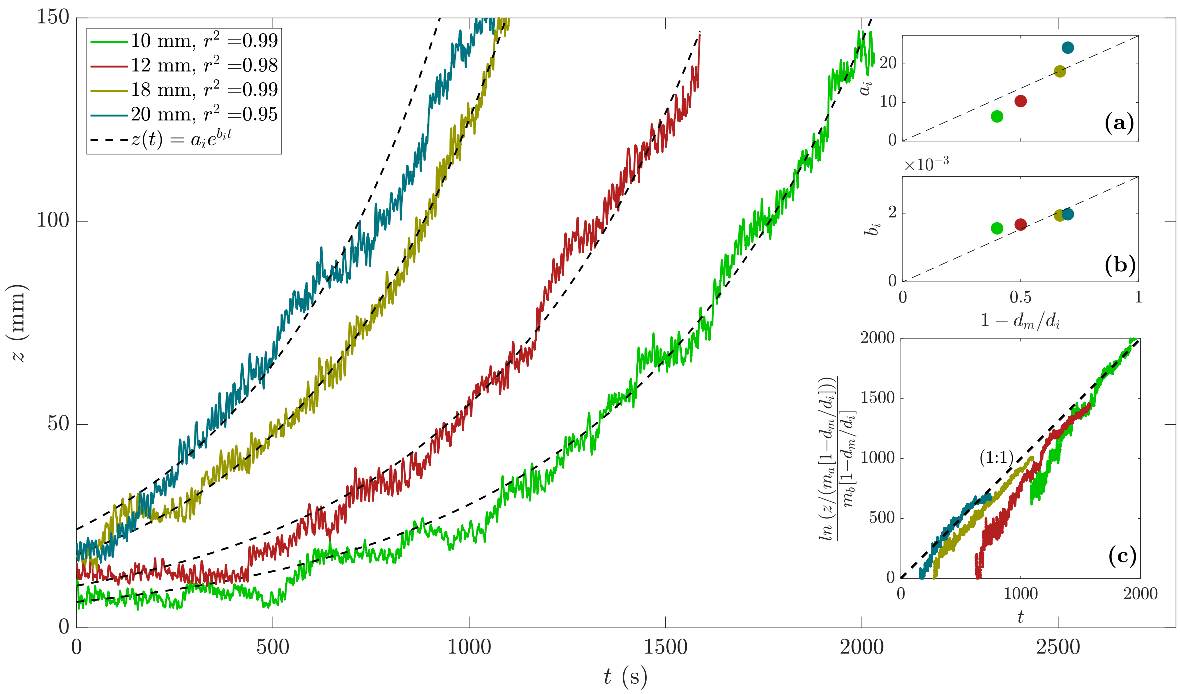

FIG. 2. Vertical position z as a function of time t for the intruders of d_i = 10, 12, 14, 18 and 20 mm in the d_m = 6 mm medium experiments. The dashed lines (---) show the exponential fits $z(t) = a_i e^{b_i t}$ with their respective correlation coefficients r^2 in the legend. (a) Linear fit for a_i as a function of $1 - d_m/d_i$ ($r^2 = 0.972$). (b) Linear fit for b_i as a function of $1 - d_m/d_i$ ($r^2 = 0.992$). (c) Experimental results collapsed, $m_a = 27.32$ and $m_b = 0.0031$ correspond to the fitted constants obtained from the upper insets.

$h = 150$ mm. Figure 3(a) shows all the normalized experimental results. Experiments with size ratios close to 0 (turquoise • and ♦) tended to a linear ascent, hence a nearly constant segregation rate. By contrast, experiments with size ratios close to 1 (green ♦ and red ★) showed strong nonlinear behavior.

To visualize all the experiments as a function of an averaged segregation rate $\overline{w}_i$, we defined this as the vertical distance h divided by t_f. This ratio neglects the nonlinear behavior shown in Figure 2, so it is different from the instantaneous segregation rate $q \approx w_i$. Figure 3(b) plots $\overline{w}_i$ as a function of $1 - d_i/d_m$. Experiments with size ratios close to 0 (turquoise • and ♦) exhibited the fastest averaged segregation rates, whereas experiments with size ratios close to 1 (green ♦ and red ★) exhibited the slowest averaged segregation rates. Figure 3(c) shows t_f as a function of $1 - d_m/d_i$. We did not observe a plateau

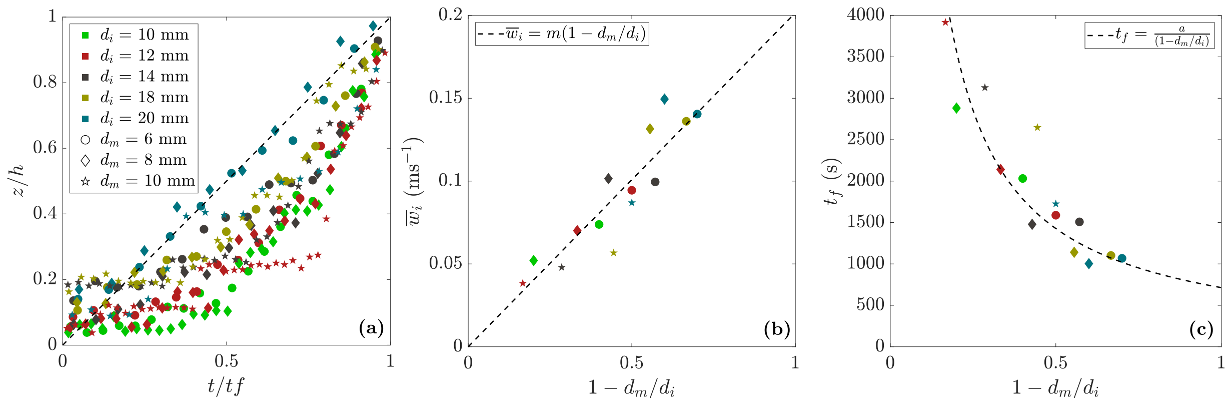

FIG. 3. (a) Normalized vertical position z/h as a function of normalized time t/t_f for all experiments. (b) Average vertical velocity $\overline{w}_i = h/t_f$ as a function of size ratio $1 - d_m/d_i$. The dashed line (---) in (b) represents a linear fit $\overline{w}_i = m(1 - d_m/d_i)$, with $m = 0.202$ ms^{-1} ($r^2 = 0.81$). (c) Final times for the segregation of intruders t_f as a function of size ratio $1 - d_m/d_i$. The dashed line (---) in (c) represents a curve fit using the expression $t_f = a/(1 - d_m/d_i)$, with $a = 713.83$ s ($r^2 = 0.76$).

for $t_f = f(1 - d_m/d_i)$, which would have indicated a constant relationship between the segregation rate and the size ratio. Neither did we find a local minimum t_f, which would have indicated a maximum segregation rate for a certain value of d_m/d_i. Our results showed a sharp increase of t_f when d_m/d_i tends to 1, especially for the experiment with $d_m/d_i = 0.833$.

B. Intruder rotation

Intruder rotation was observed as the bulk was sheared during each cycle. In some experiments the intruder rotated more, especially when intruder sizes were close to those of the media. Rotational movement did not tend towards any particular direction, and it was not necessarily synchronized with plate movement. In some cases we observed that the intruder upwards movement occurred simultaneously with its rotation.

Dot positions relative to the intruder's position are shown in Figure 4. The red dot on the intruder's circumference is plotted relative to the intruder position. Figure 4 shows that intruder rotation was highest for size ratios close to 1. For example, the $d_i = 10$ mm intruder surrounded by $d_m = 6$ mm disks rotated around its center several times, which was reflected

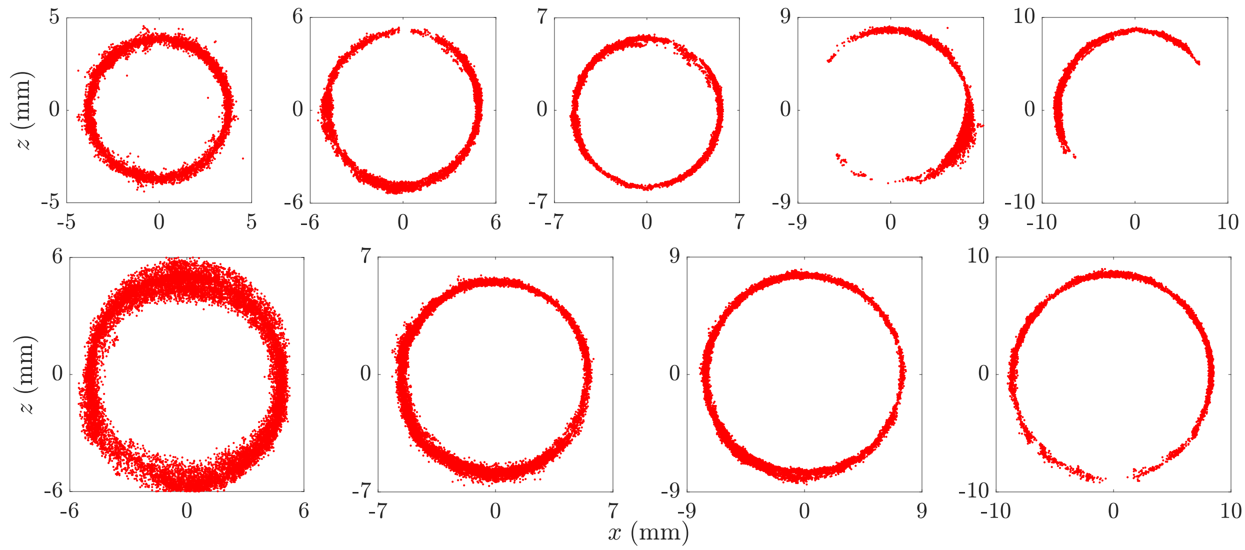

FIG. 4. Dot positions relative to the intruder's position. Top row (left to right): experiments using a $d_m = 6$ mm medium, with $d_i = 10$, 12, 14, 18 and 20 mm intruders. Bottom row (left to right): experiments using a $d_m = 10$ mm medium, with $d_i = 12$, 14, 18 and 20 mm intruders.

by the fact that the red dot's trajectory drew a complete circumference (Fig. 4 - top row, left-hand panel). Whereas smaller intruders completed several revolutions, larger intruders sometimes could not even complete one. A $d_i = 20$ mm intruder surrounded by $d_m = 6$ mm disks barely rotated. In this case the red dot was never oriented downwards or to the left of the intruder's center (Fig. 4 - top row, right-hand panel). Experiments using the $d_m = 10$ mm intruder showed the same tendency with one difference. In comparison, the same $d_i = 20$ mm intruder dot covered more of the circumference: hence this behavior was size-ratio dependent. These results indicated that in experiments with d_m/d_i closer to 1, segregation relied much more on rotation. The less active rotation observed in experiments with $d_m/d_i < 0.5$ suggested that they relied on other mechanisms to segregate.

We tracked these dots through time to measure rotation magnitudes. As explained in §II B we estimated the intruder's angular velocity ω_i and angular acceleration α_i. Figure 5 shows that both ω_i and α_i were slightly correlated to vertical velocity $w_i = dz/dt$ which approximates to the segregation rate q (Fig. 5). Another interesting feature was the increasing values of α_i as intruders rose. This increment was especially relevant for size ratios tending to unity as observed in Figure 5, where we saw higher magnitudes for α_i and a tendency for even higher α_i values as the intruder approached the free surface. We suspect that the higher α_i values reached at the end of the experiment were a consequence of lower local confinement.

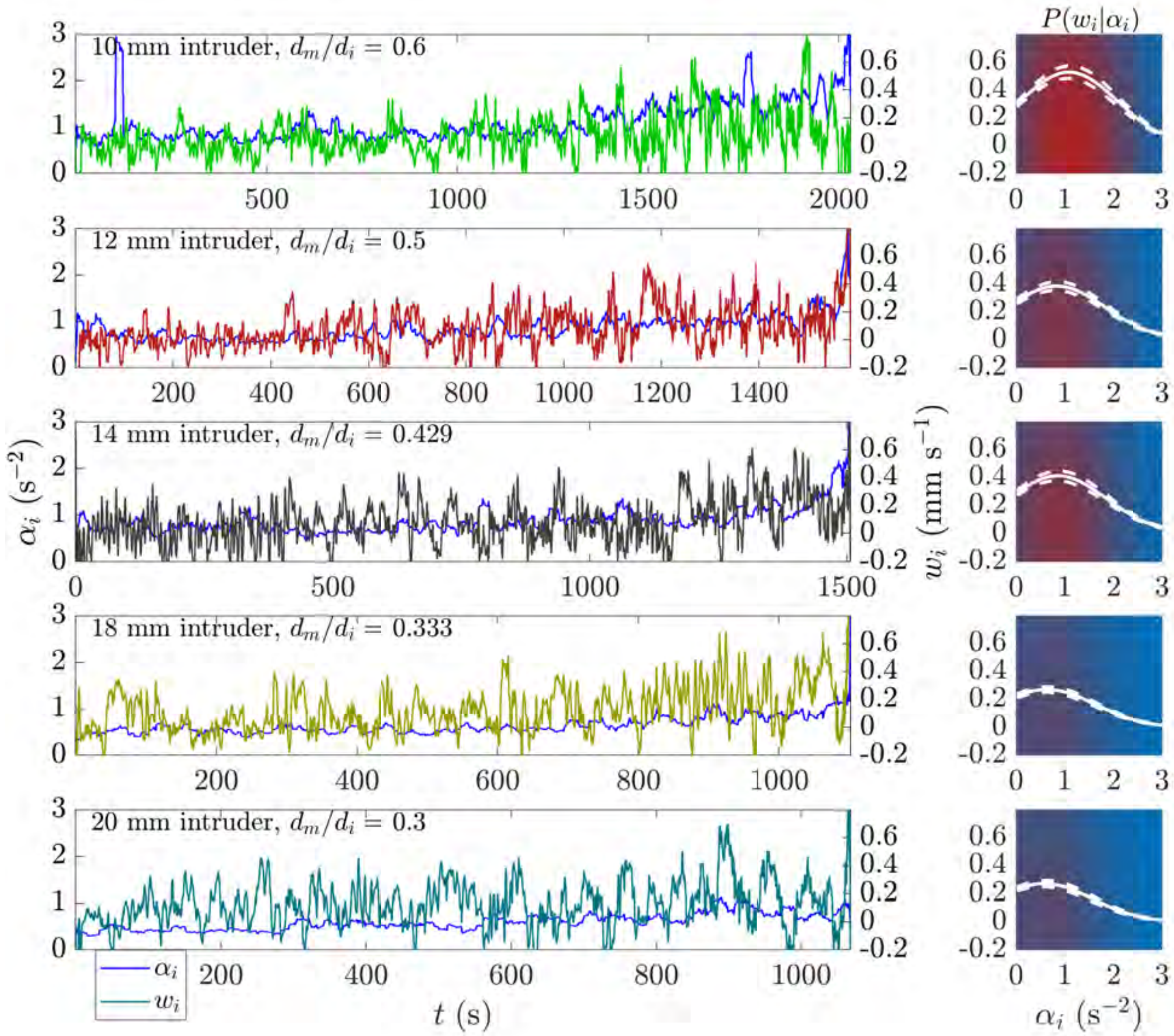

FIG. 5. Left column: intruders' angular acceleration α_i (left axis - blue line) and vertical velocities w_i (right axis, different colors) as a function of time t for experiments using the $d_m = 6$ mm medium and intruders of diameters $d_i = 10$, 12, 14, 18 and 20 mm (size ratios $d_m/d_i = 0.6$, 0.5, 0.429, 0.33 and 0.3). Right column: probability of w_i given that α_i, $P(w_i|\alpha_i)$. Red tones indicate a higher probability, with a maximum value of 0.7, and blue tones indicate a lower probability, with minimum value of 0. The continuous white line draws the mean values and the dashed white lines draw the mean values plus and minus standard deviations.

To illustrate the link between rotation and segregation, Figure 5 plots their conditional probabilities $P(w_i|\alpha_i)$. As detailed in §II B, $P(w_i|\alpha_i)$ expresses the probability that the intruder moved vertically upwards given that it rotated (Fig. 5 - right column). Experiments with $d_m/d_i > 0.4$ indicate higher probabilities that the intruder segregated given that it had rotated. Conversely, when $d_m/d_i < 0.4$, probabilities that the intruder segregated given it had rotated were lower. For each run, the probabilities of having a certain α_i value were averaged and plotted (Fig. 5 - white lines over colormaps). These averages and deviations were calculated to highlight the magnitude differences between runs with different size ratios. These results confirmed that as size ratios approach to 0, intruders have lower probabilities of segregating given that they rotated, and their rotation was weaker than that observed for size ratios tending to 1.

Figure 5 shows that, in general, α_i showed greater variability for $d_m/d_i > 0.4$ experiments. The experiment with $d_m/d_i = 0.3$ displayed the highest mean values for rotation, with a maximum at $\alpha_i \sim 3$ s^{-2}. For the rest of the experiments, their maximum values for α_i decreased as size ratio decreased to 0, as well as their conditional probabilities.

C. Strain rate tensor invariants

The first and second invariants of the strain rate tensor were calculated according to §II C. A field of each invariant was obtained for each experimental time step. Since we also knew the position of the intruder's circumference, we extracted the values of I_D and $II_{\boldsymbol{D}}$ around the intruder's circumference. As a result, the strain-rate tensor invariants $I_{\boldsymbol{D}i}$ and $II_{\boldsymbol{D}i}$ along the intruder's circumference can be plotted as functions of the intruder's arc angle ϕ_i. This angle was measured counter-clockwise from the horizontal direction towards the right of the cell (3 o'clock). To represent the experimental results of $I_{\boldsymbol{D}i}$ and $II_{\boldsymbol{D}i}$, we took their time-averaged values over the entire experiment.

Figure 6 shows the strain rate tensor invariants around the intruder's circumference, using both cartesian and polar coordinates (Fig. 6 - left and right column, respectively). In general, the mean values for both invariants depended on the size ratio. A second general observation was that $I_{\boldsymbol{D}i}$ and $II_{\boldsymbol{D}i}$ were greatest on the upper half of the intruder's circumference, in accordance with the observed upward movement. All experiments showed maximum values at $\pi/2$ and minimum values at $3\pi/2$ for both invariants. In average, greater values are found on the upper half the intruder and smaller values are found on its lower half. These results showed that the intruder moved towards regions where $I_{\boldsymbol{D}i}$ and $II_{\boldsymbol{D}i}$ were greater, thus to the free surface.

Dilation $I_{\boldsymbol{D}i}$ tended to be positive between 0 and π and negative elsewhere (contraction). For $d_m/d_i = 0.833$, the arc where $I_{\boldsymbol{D}i} > 0$ is particularly narrow (between $\pi/8$ and $3\pi/4$). This result suggests that for size ratios close to 1, gap formation was limited due to weak size heterogeneity. On the contrary, for $d_m/d_i = 0.3$, $I_{\boldsymbol{D}i}$ is positive almost anywhere around the intruder's circumference. Grain movement creates dilation and segregation is enhanced. This grain movement resulted in faster intruder velocity, a result shown in Figure 3(b). The contraction measured below the intruder, explains why large particles had difficulties to move to the cell's bottom.

Shear-rate magnitudes for each experiment depended on d_m/d_i as well. The values of $II_{\boldsymbol{D}i}$ were always positive, with its highest values observed between 0 and π, and its local maximum also at $\pi/2$. Surprisingly, size ratios close to 1 showed higher $II_{\boldsymbol{D}i}$ values. However, this observation was consistent with the argument that rotation and angular acceleration play a role in the segregation of large particles. Shear rate is related to angular deformation, which was observed experimentally by intruder rotation. The magnitudes of $II_{\boldsymbol{D}i}$ are of the same order of magnitude as the average external shear rate $\bar{\dot{\gamma}}_e = 2.67 \times 10^{-2}$ s^{-1} (Eq. 1). Even though all the experiments shared the same externally imposed shear rate, $II_{\boldsymbol{D}i}$ was locally distributed around the intruder's circumference at values ranging between approximately 1.8×10^{-2} and 2×10^{-2} s^{-1} (Fig. 6). Also, the mean values of $II_{\boldsymbol{D}i}$ around the intruder's circumference are dependent on the size ratio. These mean values show differences of 6×10^{-3} s^{-1} between the experiments with size ratios of 0.833 and 0.3 (Figure 6 - red ★ and turquoise •, respectively).

Figure 6 also presents two intermediate cases with $d_m/d_i = 0.5$ for particle diameters of 6 and 10 mm, and intruders of 12 and 20 mm, respectively. Even though the size ratios are the same, the values calculated for $I_{\boldsymbol{D}i}$ and $II_{\boldsymbol{D}i}$ were different, with mean differences of 1×10^{-3} and 2×10^{-4} s^{-1}, respectively. We think these differences were due to the plate roughness and slightly different W/d_m values.

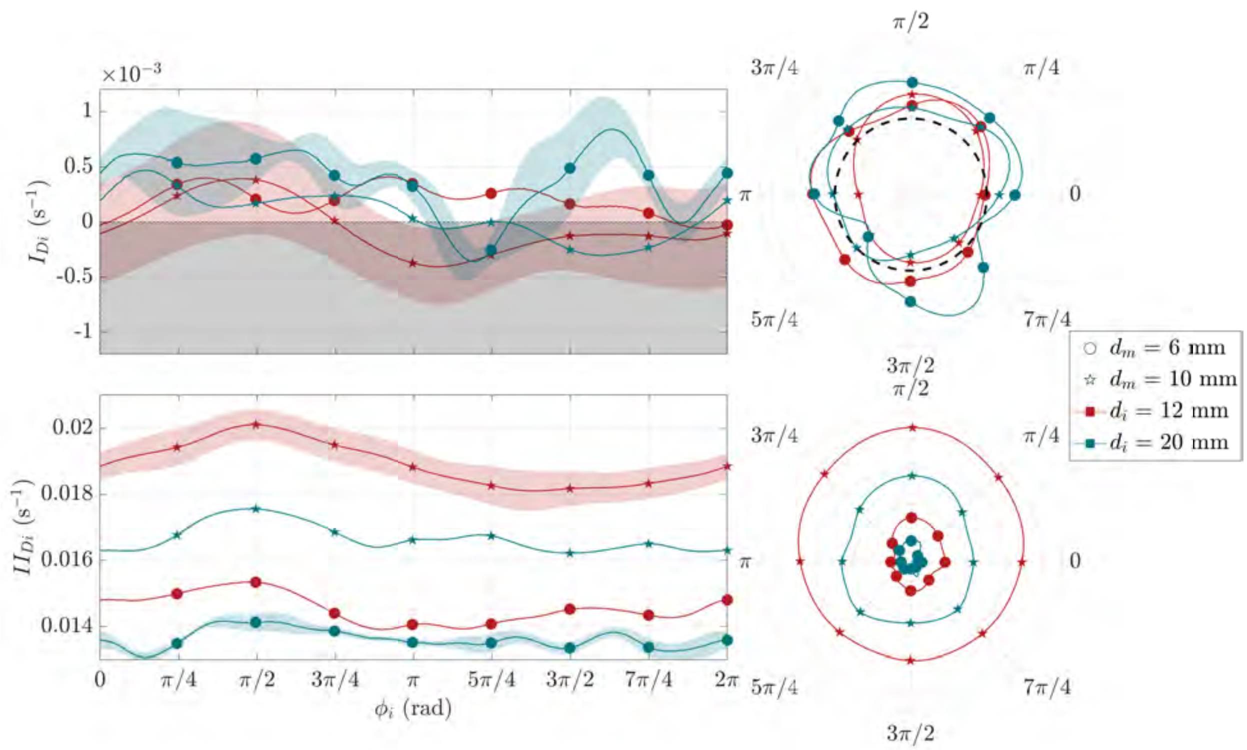

FIG. 6. Left column. Time-averaged strain rate-tensor invariants for dilation $I_{\boldsymbol{D}i}$ (top row) and shear rate $II_{\boldsymbol{D}i}$ (bottom row), around the intruder's circumference ϕ_i, with the angle measured counter-clockwise from the horizontal direction towards the right of the cell (3 o'clock). Colored areas represent values and their standard deviation. The gray area represents contraction. Right column. Polar plots of the same strain rate-tensor invariants for the experiments with $d_m = 6$ (•) and 10 (★) mm media, and $d_i = 12$ (red) and 20 (turquoise) intruders. Standard deviations were not plotted for all experiments for visualization purposes.

D. Segregation mechanism

Even though the *squeeze expulsion* mechanism was largely well-described by Savage and Lun [1], they provided no clear role for the particles' size ratio. Our results in §III suggest that segregation is caused by a combination of dilation and rotation that depends on size ratio d_m/d_i. Dilation was predominant for d_m/d_i values closer to zero and segregation rates were faster in these cases. Dilation faded as d_m/d_i increased, but segregation still happened. For d_m/d_i tending to 1, rotation and shear rate became predominant, and they were significant for segregation. For $d_m/d_i < 0.5$, segregation rates were considerably higher; thus, dilation was a much more effective sub-mechanism for segregation than rotation was. Nonetheless, rotation's contribution for relatively smaller intruders is still key for their segregation.

Two processes occur in an initially dense granular material that undergoes shear (Figure 7 - first figure panels in both rows):

- If dilation $I_{\boldsymbol{D}}$ around the intruder is large enough, surrounding particles entrain below it. This small-particle entrainment may lift the intruder up, presumably through normal stress redistribution. This occurrence of entrainment does not depend solely on dilation. All our experiments were subjected to the same shear rate $II_{\boldsymbol{D}}$ and effective bulk height h, yet segregation rates differed (Fig. 3). Therefore, the second variable controlling the entrainment should be d_m/d_i. When $d_m/d_i < 0.5$ it becomes easier for disks surrounding the intruder to entrain. For d_m/d_i close to unity, entrainment is less frequent, due to weak gap generation, and the intruder usually remains in its place.

- Shear-induced dilation redistributes forces around the intruder. As a result, the intruder may become interlocked with its neighbors. Normal stresses transmitted through the intruder's neighbors create a force network that restrains the intruder's movement. When shear continues to be applied, the interlocked particles move conjointly around a pivot below them. Similarly to the first process, this rotational movement depends on d_m/d_i. Our results indicated higher rotation, a greater probability $P(w_i|\alpha_i)$, and higher local shear rates $II_{\boldsymbol{D}i}$ for $d_m/d_i > 0.5$ (Fig. 5). A size ratio close to 1 indicates that interlocking is likely to be occurring. It is plausible that slight size differences between the intruder and the medium require fewer surrounding particles to lock-in the intruder. However, our experiments showed that the probability of interlocking remains low. Therefore, the segregation caused by this process is slower and less effective than that caused by the first process.

See Supplemental Material at [URL will be inserted by publisher] for experimental videos that show the segregation mechanisms. All files related to a published paper are stored as a single deposit and assigned a Supplemental Material URL. This URL appears in the articles reference list.

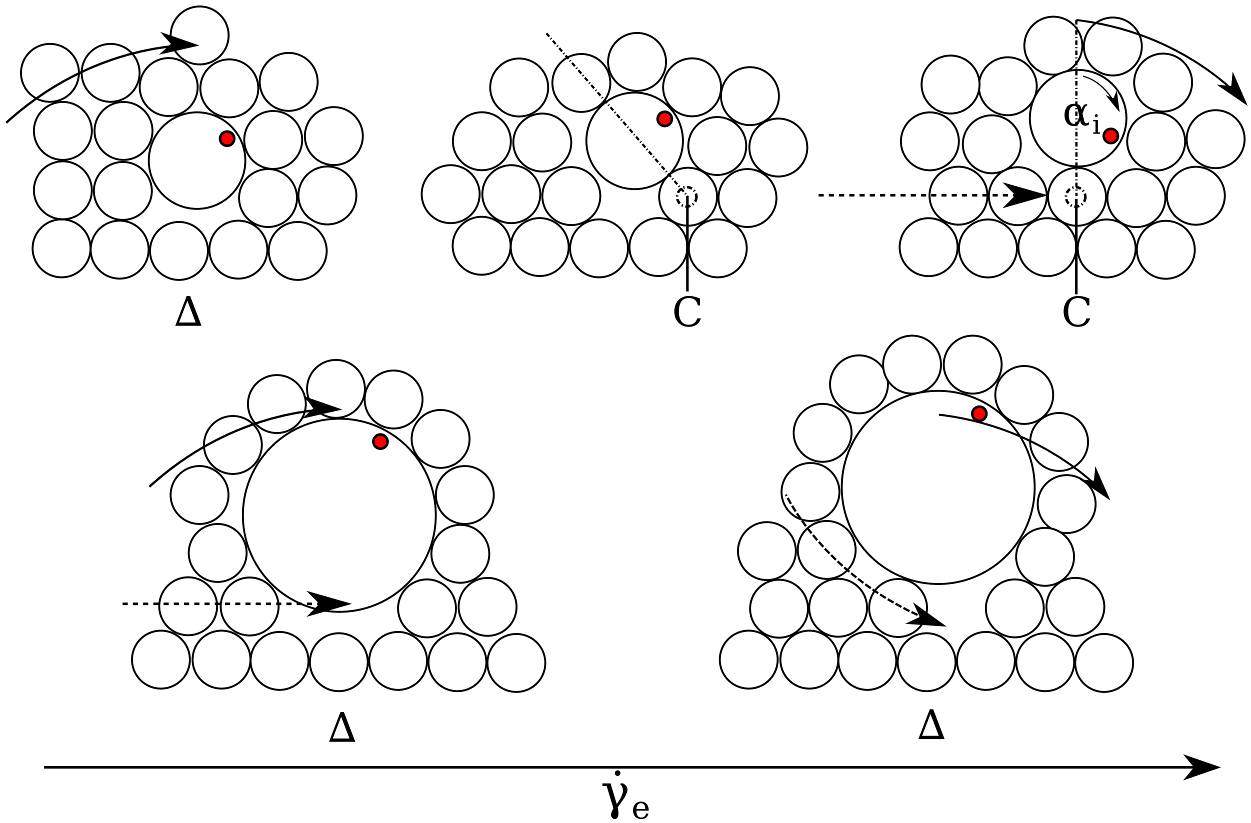

FIG. 7. Scaled schema of the segregation of a single large intruder of $d_i = 10$ (top row) and 20 (bottom row) mm under the action of an external shear rate $\dot{\gamma}_e$. Top row. Rotation-based mechanism. The bulk medium dilates (left panel - Δ) and creates a contact network that locks-in the intruder (middle panel). Further shear generates intruder rotation (represented by α_i) around the pivotal point C (right panel). Bottom row. Rotation-based mechanism. The bulk medium dilates (both panels - Δ), generating gaps for particles to slide beneath (right panel - dashed arrows). Experimental images and videos showing these mechanisms are provided as supplemental material.

IV. CONCLUSIONS

A two-dimensional, oscillatory shear-cell was used to study the segregation of a large particle intruder through a medium of smaller particles. The intruder's position and rotation were measured and tracked over time. We found that the segregation rate was a non-linear function of time, dependent on the intruder's depth and the size ratio d_m/d_i. An increase in the size ratio decreased the segregation rate. Intruder rotation, quantified in terms of angular acceleration, was found to be more frequent and intense, the close the size ratio is to 1. We conclude that intruder rotation is a relevant mechanism in the segregation of large particles, in agreement with the proposition of Jing *et al.* [28].

Using a different setup and flow configuration, we found the same segregation behavior as that presented by several authors [22, 24, 40], large particles segregated, predominantly, towards regions where dilation was greater. Complementarily, we found that for size ratios close to 1 shear rate becomes a relevant variable for segregation. The shear-rate gradient causes the intruder to rotate, resulting in its segregation; thus, intruders may also segregate towards more sheared regions. Even though we did not present stress measurements, we presented a plausible explanation for the role of the local shear-stress gradient in the segregation of large particles.

Based on the observations presented here, we have suggested a detailed description of the *squeeze expulsion* mechanism, the variables and the processes affecting it. The first process is strongly dependent on dilation, whereas the second depends on rotation, i.e., represented by the shear rate. Frustration of the rotation-based process depends on surrounding interparticle contacts, which was observed for $d_m/d_i < 0.5$ where the intruder needed more particles in close contact to interlock. We proposed that the occurrence of these processes, although independent of each other, are highly dependent on the size ratio.

ACKNOWLEDGMENTS

We acknowledge the support of the Swiss National Science Foundation through Project 200020_175750. We are grateful for the support from the Swiss Federal Commission for Scholarships and we acknowledge the initial support from the Comisión Nacional de Ciencia y Tecnología (CONICYT). This research was supported by NERC grants NE/E003206/1 and NE/K003011/1 as well as EPSRC grants EP/I019189/1, EP/K00428X/1 and EP/M022447/1. J.M.N.T.G. is a Royal Society Wolfson Research Merit Award holder (WM150058) and an EPSRC Established Career Fellow (EP/M022447/1).

We would also like to thank Bob de Graffenried for his technical support and advice.

---

[1] S. B. Savage and C. Lun, Particle size segregation in inclined chute flow of dry cohesionless granular solids, Journal of Fluid Mechanics **189**, 311 (1988).

[2] H. A. Makse, S. Havlin, P. R. King, and H. E. Stanley, Spontaneous stratification in granular mixtures, Nature **386**, 379 (1997).

[3] O. Pouliquen, J. Delour, and S. B. Savage, Fingering in granular flows, Nature **386**, 816 (1997).

[4] M. Woodhouse, A. Thornton, C. Johnson, B. Kokelaar, and J. M. N. T. Gray, Segregation-induced fingering instabilities in granular free-surface flows, Journal of fluid mechanics **709**, 543 (2012).

[5] R. M. Iverson, The physics of debris flows, Reviews of geophysics **35**, 245 (1997).

[6] G. Félix and N. Thomas, Relation between dry granular flow regimes and morphology of deposits: formation of leves in pyroclastic deposits, Earth and Planetary Science Letters **221**, 197 (2004).

[7] T. Takahashi, Debris flow, Annual Review of Fluid Mechanics **13**, 57 (1981), https://doi.org/10.1146/annurev.fl.13.010181.000421.

[8] I. F. Denissen, T. Weinhart, A. Te Voortwis, S. Luding, J. Gray, and A. Thornton, Bulbous head formation in bidisperse shallow granular flow over an inclined plane, Journal of Fluid Mechanics **866**, 263 (2019).

[9] A. Mangeney, F. Bouchut, N. Thomas, J.-P. Vilotte, and M. Bristeau, Numerical modeling of self-channeling granular flows and of their levee-channel deposits, Journal of Geophysical Research: Earth Surface **112** (2007).

[10] B. Kokelaar, R. Graham, J. M. N. T. Gray, and J. Vallance, Fine-grained linings of leveed channels facilitate runout of granular flows, Earth and Planetary Science Letters **385**, 172 (2014).

[11] R. Delannay, A. Valance, A. Mangeney, O. Roche, and P. Richard, Granular and particle-laden flows: from laboratory experiments to field observations, Journal of Physics D: Applied Physics **50**, 053001 (2017).

[12] T. Shinbrot, Granular materials: The brazil nut effectin reverse, Nature **429**, 352 (2004).

[13] H. A. Makse, Grain segregation mechanism in aeolian sand ripples, The European Physical Journal E **1**, 127 (2000).

[14] J. M. N. T. Gray and B. Kokelaar, Large particle segregation, transport and accumulation in granular free-surface flows, Journal of Fluid Mechanics **652**, 105 (2010).

[15] J. M. N. T. Gray, Particle segregation in dense granular flows, Annual Review of Fluid Mechanics (2018).

[16] J. Bridgwater, Fundamental powder mixing mechanisms, Powder Technology **15**, 215 (1976).

[17] J. C. Williams, The segregation of particulate materials. a review, Powder technology **15**, 245 (1976).

[18] A. Rosato, K. J. Strandburg, F. Prinz, and R. H. Swendsen, Why the brazil nuts are on top: Size segregation of particulate matter by shaking, Physical Review Letters **58**, 1038 (1987).

[19] G. V. Middleton, Experimental studies related to problems of flysch sedimentation, Flysch sedimentology in North America. , 253 (1970).

[20] K. M. Hill and Y. Fan, Granular temperature and segregation in dense sheared particulate mixtures, KONA Powder and Particle Journal **33**, 150 (2016).

[21] R. P. Jones, A. B. Isner, H. Xiao, J. M. Ottino, P. B. Umbanhowar, and R. M. Lueptow, Asymmetric concentration dependence of segregation fluxes in granular flows, Physical Review Fluids **3**, 094304 (2018).

[22] L. A. Golick and K. E. Daniels, Mixing and segregation rates in sheared granular materials, Physical Review E **80**, 042301 (2009).

[23] K. van der Vaart, P. Gajjar, G. Epely-Chauvin, N. Andreini, J. M. N. T. Gray, and C. Ancey, Underlying asymmetry within particle size segregation, Physical Review Letters **114**, 238001 (2015).

[24] F. Guillard, Y. Forterre, and O. Pouliquen, Scaling laws for segregation forces in dense sheared granular flows, Journal of Fluid Mechanics **807** (2016).

[25] K. van der Vaart, M. van Schrojenstein Lantman, T. Weinhart, S. Luding, C. Ancey, and A. Thornton, Segregation of large particles in dense granular flows suggests a granular saffman effect, Physical review fluids **3**, 074303 (2018).

[26] L. Staron, Rising dynamics and lift effect in dense segregating granular flows, Physics of Fluids **30**, 123303 (2018).

[27] G. Hill, S. Yeung, and S. A. Koehler, Scaling vertical drag forces in granular media, EPL (Europhysics Letters) **72**, 137 (2005).

[28] L. Jing, C. Kwok, and Y. Leung, Micromechanical origin of particle size segregation, Physical review letters **118**, 118001 (2017).

[29] Y. Ding, N. Gravish, and D. I. Goldman, Drag induced lift in granular media, Physical Review Letters **106**, 028001 (2011).

[30] F. Guillard, Y. Forterre, and O. Pouliquen, Lift forces in granular media, Physics of Fluids

26, 043301 (2014).

[31] A. Seguin, C. Coulais, F. Martinez, Y. Bertho, and P. Gondret, Local rheological measurements in the granular flow around an intruder, Physical Review E **93**, 012904 (2016).

[32] A. Drescher and G. D. J. De Jong, Photoelastic verification of a mechanical model for the flow of a granular material, Journal of the Mechanics and Physics of Solids **20**, 337 (1972).

[33] A. Scott and J. Bridgwater, Self-diffusion of spherical particles in a simple shear apparatus, Powder Technology **14**, 177 (1976).

[34] D. Stephens and J. Bridgwater, The mixing and segregation of cohesionless particulate materials part ii. microscopic mechanisms for particles differing in size, Powder Technology **21**, 29 (1978).

[35] *MATLAB version 9.6.0.1099231 (R2019a)*, The Mathworks Inc., Natick, Massachusetts (2019).

[36] J. C. Crocker and D. G. Grier, Methods of digital video microscopy for colloidal studies, Journal of colloid and interface science **179**, 298 (1996).

[37] S. P. Timošenko and J. Goodier, *Theory of elasticity*, third ed., 23rd print., [international ed.] ed., McGraw-Hill international editions. Engineering mechanics series (McGraw-Hill Book, Auckland, 1988).

[38] L. D. Landau and E. M. Lifšic, *Theory of elasticity*, 3rd ed., Course of theoretical physics, Vol. vol. 7 Ed.3 (Butterworth-Heinemann, Oxford, 1999).

[39] B. Andreotti, Y. Forterre, and O. Pouliquen, *Granular media: between fluid and solid* (Cambridge University Press, 2013).

[40] S. Wiederseiner, N. Andreini, G. Épely-Chauvin, G. Moser, M. Monnereau, J. M. N. T. Gray, and C. Ancey, Experimental investigation into segregating granular flows down chutes, Physics of Fluids **23**, 013301 (2011).